Involvement of the cysteine-rich head domain in activation and desensitization of the P2X1 receptor

Éva Lörinczi[a,1], Yogesh Bhargava[b,2], Stephen F. Marino[b,c,2,3], Antoine Taly[d,2], Karina Kaczmarek-Hájek[a], Alonso Barrantes-Freer[a], Sébastien Dutertre[e], Thomas Grutter[d], Jürgen Rettinger[b], and Annette Nicke[a,c,4]

[a]Department of Molecular Biology of Neuronal Signals, Max Planck Institute for Experimental Medicine, 37075 Göttingen, Germany; [b]Department of Biophysical Chemistry, Max Planck Institute for Biophysics, 60438 Frankfurt, Germany; [c]Department of Neurochemistry, Max Planck Institute for Brain Research, 60528 Frankfurt, Germany; [d]Laboratoire de Biophysicochimie des Récepteurs Canaux, Unité Mixte de Recherche 7199 Faculté de Pharmacie—Université de Strasbourg, 67401 Illkirch, France; and [e]Institute for Molecular Bioscience, University of Queensland, Brisbane QLD 4072, Australia

P2X receptors (P2XRs) are ligand-gated ion channels activated by extracellular ATP. Although the crystal structure of the zebrafish P2X4R has been solved, the exact mode of ATP binding and the conformational changes governing channel opening and desensitization remain unknown. Here, we used voltage clamp fluorometry to investigate movements in the cysteine-rich head domain of the rat P2X1R (A118-I125) that projects over the proposed ATP binding site. On substitution with cysteine residues, six of these residues (N120–I125) were specifically labeled by tetramethyl-rhodamine-maleimide and showed significant changes in the emission of the fluorescence probe on application of the agonists ATP and benzoyl-benzoyl-ATP. Mutants N120C and G123C showed fast fluorescence decreases with similar kinetics as the current increases. In contrast, mutants P121C and I125C showed slow fluorescence increases that seemed to correlate with the current decline during desensitization. Mutant E122C showed a slow fluorescence increase and fast decrease with ATP and benzoyl-benzoyl-ATP, respectively. Application of the competitive antagonist 2′,3′-O-(2,4,6-trinitrophenyl)-ATP (TNP-ATP) resulted in large fluorescence changes with the N120C, E122C, and G123C mutants and minor or no changes with the other mutants. Likewise, TNP-ATP–induced changes in control mutants distant from the proposed ATP binding site were comparably small or absent. Combined with molecular modeling studies, our data confirm the proposed ATP binding site and provide evidence that ATP orients in its binding site with the ribose moiety facing the solution. We also conclude that P2XR activation and desensitization involve movements of the cysteine-rich head domain.

P2X receptors (P2XRs) represent a family of nonselective cation channels gated by extracellular ATP. They are widely distributed in mammalian tissues and have been shown to be involved in diverse physiological functions (1). The seven known subunits all contain two transmembrane domains linked by a large extracellular loop. Functional receptors are homo- or heteromeric trimers (2, 3).

Based on mutagenesis studies, it has been suggested that conserved positively charged and aromatic residues are crucial for ATP binding, presumably by interacting with the negatively charged phosphate chain of ATP (4–6) and its adenine ring (6), respectively. We have previously shown that replacement of two of these residues, K68 and F291, by cysteine residues allows disulfide cross-linking between neighboring P2X1 subunits and that this reaction is prevented in the presence of ATP. Based on these data, we concluded that the ATP binding sites are located at the subunit interfaces (7, 8). This conclusion is in good agreement with the positions of the relevant amino acids in the crystal structure of the unliganded P2X4R from zebrafish (2). This zP2X4 structure revealed an ion channel architecture that resembles a dolphin, with the transmembrane helices and the extracellular region forming the fluke and the upper body, respectively. Attached to the body domain, a head domain, a dorsal fin, and right and left flippers have been defined. It was suggested that the ATP binding site is formed by deep intersubunit grooves, which are surrounded by the conserved residues implicated in ATP binding. These residues are provided by the body domain and enclosed by the left flipper of one subunit and the dorsal fin of the neighboring subunit. The cysteine-rich head domain of the first subunit projects over this binding site (2). Because the zP2X4 crystal was obtained in the absence of ATP, the exact mode of agonist binding is unknown. Likewise, the conformational changes governing channel opening and desensitization remain elusive.

A powerful method for resolving ligand interactions and structural rearrangements accompanying the conformational transitions of channels and transporters is the simultaneous recording of current responses and fluorescence changes after site-directed fluorescence labeling by voltage clamp fluorometry (VCF) (9). This method has the potential to detect electrically silent processes, such as antagonist binding or recovery from desensitization. A common structural feature of all vertebrate P2XRs is five conserved disulfide bridges. Three of these disulfide bridges are arranged in the head domain (2). Two findings suggest a close association of this region with ATP binding: (i) the P2X7 subtype has been found to be constitutively active on ADP ribosylation of residue R125 located between the first and second conserved cysteine residues (10), and (ii) a recent report has shown that the thiol-reactive ATP analog 8-thiocyano-ATP (NCS-ATP) can be covalently attached to the cysteine-substituted residue N140C in the head domain of the P2X2R (11). To probe the proximity of the first intercysteine region to the presumed ATP binding site and a possible function of the cys-rich region in receptor activation and/or desensitization, we performed VCF with the fast desensitizing P2X1R expressed in *Xenopus* oocytes. Our data reveal details about the implication of the cys-rich head domain in ligand binding, channel activation, and desensitization of the P2X1R.

Results

Generation and Assembly of Cysteine-Substituted P2X1 Receptor Mutants. Each of the eight residues in the first intercysteine region (positions A118 to I125) was exchanged by a cysteine residue in the hexahistidyl-tagged rat P2X1R. To ensure that the mutant receptors were correctly folded and functional, our mutations were done on the background of the naturally occurring 10 cysteine residues. Because this process bears the risk of receptor misfolding due to unspecific disulfide cross-linking, we first analyzed the efficiency of surface expression of each mutant by selective labeling of the resulting plasma membrane receptors with Cy5-conjugated N-hydroxysuccinimide ester (7), which reacts with primary amines at the cell surface. As shown by SDS/PAGE analysis in Fig. 1A,

all mutants generated uniform receptor populations with expression levels in the plasma membrane that were similar to the levels of the WT receptor or even higher, showing that the introduced cysteine residues did not notably influence receptor folding, assembly, or surface transport (Table S1). In addition, two-electrode voltage clamp analysis of the mutants and WT receptors revealed similar EC_{50} values (at most, a 10-fold difference) for ATP, further confirming that the introduced cysteine residues did not severely affect receptor function (Fig. 1C and Table S2).

Identification of Tetramethyl-Rhodamine-Maleimide–Accessible Residues in the Cys-Rich Extracellular Domain. We next used VCF to monitor the changes in fluorescence intensities of single fluorescent probes that are specifically attached to free cysteine residues. To identify residues that are accessible, we incubated all cysteine mutants with the sulfhydryl-reactive fluorescent dye tetramethyl-rhodamine-maleimide (TMRM). As depicted in Fig. 1B, no labeling was observed with the WT P2X1R, confirming that all endogenous cysteine residues are oxidized or buried within the protein (2, 12, 13). In contrast, six of eight cysteine substitutions were specifically labeled by TMRM. TMRM labeling did not notably change the ATP sensitivity of the mutants (Table S2), indicating that the modifications do not impose any steric hindrance with ATP or residues involved in receptor activation or that the flexible linker allows the required movements. It has to be noted, however, that small changes in binding affinity would not lead to changes in the EC_{50} value because of the fast and long-lasting desensitization (14).

Different Positions in the C1–C2 Intercysteine Stretch Sense Different Changes in Fluorophore Environment. Simultaneous recording of current responses and fluorescence on application of 10 μM ATP showed pronounced fluorescence changes of between 2.7% and 6.1% upon receptor activation in all labeled mutants (Table S3). Based on their directions and time courses, the fluorescence changes could be divided into three groups. Mutants N120C and G123C showed a decrease in fluorescence on ATP application, and these fluorescence changes were fast and seemed to be complete when peak currents where reached (Fig. 2A). Mutant G124C showed a fast fluorescence increase (Fig. 2A). Mutants P121C, E122C, and I125C displayed slower ATP-induced fluorescence increases that reached a steady state only several seconds after the peak current response (Fig. 2B). A small initial fluorescence decrease generally preceded this signal (Fig. S1A, arrows). After the washout of ATP, the fluorescence signals of all mutants did not significantly revert within a recording time of 50 s (Fig. S1), even if only short pulses of ATP were applied (Fig. S2A). This finding is in agreement with both slow unbinding of ATP and an extremely slow recovery from desensitization as previously determined (14). Because bleaching of the fluorophore and slow fluorescence run-up/run-down effects biased longer recordings, the reversibility of the fluorescence changes was not further investigated. However, the P2X1 E122C mutant showed a slow reversibility, and the T123C (analogous to I125C in P2X1) mutant of the nondesensitizing P2X2R revealed a completely reversible fluorescence signal (Fig. S2B), thus arguing against an irreversible effect of TMRM.

Analysis of emission spectra before and after application of ATP revealed superimposable spectra in all mutants, thus excluding that the fluorescence changes were caused by a shift in the TMRM emission spectrum (Fig. S3).

Fluorescence Changes in Mutants N120C and G123C Are Associated with Receptor Activation. To better correlate kinetics of fluorescence changes observed with receptor activation or desensitization, we determined the time constants for the current and fluorescence changes (Table S3). With WT and all mutant receptors, activation time constants between 0.1 ± 0.03 and 1 ± 0.01 s were obtained for the current responses. The respective desensitization kinetics were, in most mutants, best fitted by a biexponential function, with faster and slower time constants ranging from 0.4 ± 0.1 to 2.3 ± 0.4 s and from 2.9 ± 0.4 to 8.3 ± 1.1 s, respectively. Notably, however, the time constants of the fluorescence changes seen with the N120C, G123C, and G124C mutants were more similar (0.3 ± 0.1, 0.4 ± 0.04, and 0.3 ± 0.1 s, respectively) to the activation time constants, whereas in case of the P121C, E122C, and I125C mutants, they correlated better with the current desensitization constants. Similar results were obtained when receptors were activated with 10 μM ATP-γS (Table S3). We conclude from these data that the N120C, G123C, and G124C mutants report ligand binding and/or conformational changes during channel opening, whereas the other mutants report structural rearrangements that are more likely associated with subsequent processes, such as receptor desensitization. In support of this interpretation, current and fluorescence changes start at virtually identical times after ATP application to the N120C, G123C, and G124C mutants, whereas fluorescence changes begin with a 200- to 300-ms delay (compared with the current) in mutants P121C, E122C, and I125C (Fig. 2C).

Mutant E122C Specifically Senses Binding of Benzoyl-Benzoyl-ATP. To further support this hypothesis, we repeated the above experiments with the partial agonist benzoyl-benzoyl-ATP (Bz-ATP). Bz-ATP has a similar EC_{50} value as ATP but has been shown to induce currents with slower activation times than ATP (15). Here, we found about twofold slower current activation time constants for Bz-ATP compared with ATP with the N120C ($\tau_{ATP} = 0.2 \pm 0.03$ and $\tau_{Bz\text{-}ATP} = 0.5 \pm 0.04$), G123C ($\tau_{ATP} = 0.2 \pm 0.02$ and $\tau_{Bz\text{-}ATP} = 0.5 \pm 0.1$), and G124C ($\tau_{ATP} = 0.3 \pm 0.04$ and $\tau_{Bz\text{-}ATP} = 0.5 \pm 0.1$) mutants (Table S3). Likewise, the time constants of their fluorescence changes were about twofold slower (N120C: $\tau_{ATP} = 0.3 \pm 0.1$, $\tau_{Bz\text{-}ATP} = 0.6 \pm 0.04$; G123C: $\tau_{ATP} = 0.4 \pm 0.04$, $\tau_{Bz\text{-}ATP} = 0.8 \pm 0.2$; G124C: $\tau_{ATP} = 0.3 \pm 0.1$, $\tau_{Bz\text{-}ATP} = 0.8 \pm 0.1$), supporting the close association of their fluorescence changes with the channel activation process. Unexpectedly, if activated by Bz-ATP, the fluorescence change of mutant E122C was reversed from a slowly increasing ($\tau_1 = 2.4 \pm 0.4$, $\tau_2 = 19.2 \pm 1.3$) to a fast decreasing ($\tau_1 = 0.9 \pm 0.2$) signal that seemed to be more closely associated with the time course of current activation (Fig. 2 B and D). This reversal of fluorescence change was accompanied by a threefold increase in the amplitude of the fluorescence change from $3.9 \pm 0.5\%$ on activation with ATP to $12.4 \pm 1.7\%$ with Bz-ATP. The specificity and amplitude
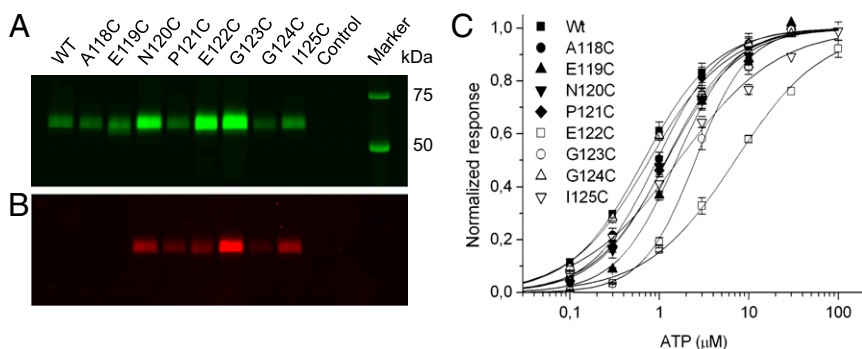

Fig. 1. Surface expression, TMRM labeling and functional analysis of cysteine-substituted mutants. The indicated His-P2X1 constructs were expressed in *Xenopus* oocytes and successively labeled with the (A) amino-reactive fluorescence dye Cy5 (labeling of surface protein) and (B) TMRM. P2X complexes were purified by Ni^{2+}-NTA agarose and separated by SDS/PAGE. Gels were directly scanned with a fluorescence scanner. Statistical analysis is in Table S1. (C) Normalized dose–response curves for ATP of WT and single cysteine mutant receptors. Lines represent nonlinear curve fits of the Hill equation to the data (for EC_{50} values and Hill coefficients) (Table S2). Error bars represent SE of 5–11 experiments.
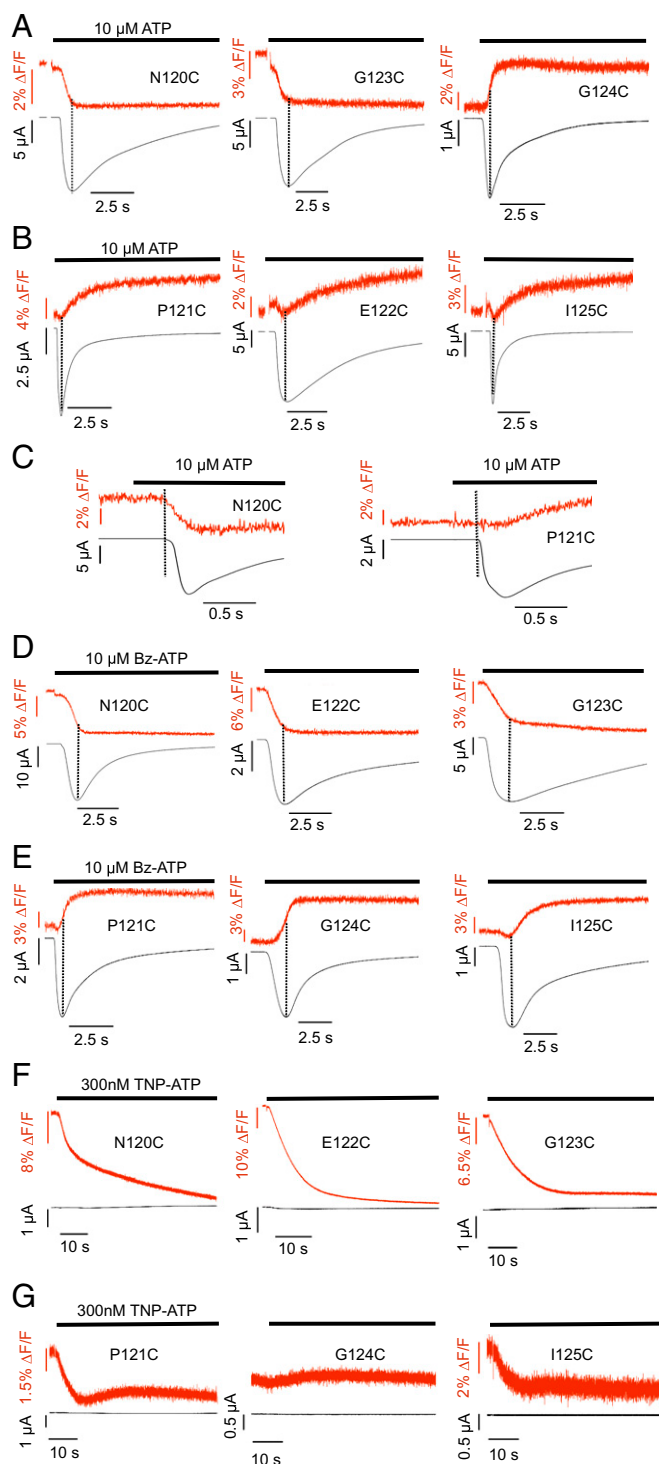
PHARMACOLOGY

Fig. 2. Comparison of current traces and fluorescence changes induced by ATP and ATP analogs. TMRM-labeled oocytes expressing the indicated His-P2X1 cysteine mutants were analyzed by VCF at −60 mV. Representative recordings of simultaneous current and fluorescence traces are shown for (*A–C*) 10 μM ATP, (*D* and *E*) 10 μM Bz-ATP, and (*F* and *G*) 300 nM TNP-ATP. (*C*) Representative recordings at an expanded time scale to show the latency between the start of current and fluorescence changes. Dotted lines indicate current peak times or current onset (*C*).

of this fluorescence change suggest that the TMRM attached to E122C interacts with the Bz moiety of Bz-ATP and thus, at least partially, reports binding of Bz-ATP.

Use of the Competitive Antagonist 2′,3′-O-(2,4,6-trinitrophenyl)-ATP Confirms that Mutants N120C, E122C, and G123C Report Ligand Binding. To further differentiate whether the fluorescence changes were reporting ATP binding or subsequent conformational changes, we made use of the competitive P2X1R antagonist 2′,3′-O-(2,4,6-trinitrophenyl)-ATP (TNP-ATP) that can be expected to have a similar binding mode as ATP (16). If the agonist-induced fluorescence changes resulted from conformational changes associated with channel opening or desensitization, no fluorescence changes would be expected with TNP-ATP, because it does not induce opening. As seen in Fig. 2*F*, TNP-ATP caused large fluorescence decreases for the N120C (20.3 ± 2.1%), E122C (43.4 ± 2.5%), and G123C (13.5 ± 1.7%) mutants. Interestingly, the direction and rank order of fluorescence amplitudes mirrored the direction and rank order of Bz-ATP–induced fluorescence amplitudes for these mutants: E122C (12.4 ± 1.7%) > N120C (9.6 ± 0.7%) > G123C (5.4 ± 0.6%) (Table S3). In contrast, mutants P121C (3.7 ± 0.2%), G124C (0%), and I125C (2.3 ± 0.3%) showed comparably small or no TNP-ATP–induced fluorescence changes (Fig. 2*G*). To test if the large fluorescence changes are caused by a direct TMRM–ligand interaction, we generated Stern–Volmer plots for the ligands and *N*-acetyl-L-tryptophanamide(NATA), which was used as a model for an amino acid with a strong quenching efficiency (Fig. S4). The obtained quenching efficiencies (ATP < NATA < Bz-ATP < TNP-ATP) correlated with the fluorescence amplitudes of the ligands at the individual mutants, and the higher efficiencies of Bz-ATP and TNP-ATP compared with NATA are in line with a direct interaction between Bz-ATP and TNP-ATP with TMRM. However, the absence of quenching by ATP indicates that fluorescence changes observed with ATP report protein movements rather than direct ligand interaction.

Fluorescence Changes in Residues P121C, E122C, and I125C Are Associated with Receptor Desensitization. After opening of the ion channel pore, the P2X1R is believed to undergo conformational changes that lead to the closed desensitized state. Because the fluorescence changes in mutants P121C, E122C, and I125C started when the current response reached its maximum and saturated only clearly after the current peak, we supposed that they were associated with the desensitization process. However, the time constants of desensitization and the respective fluorescence changes seemed more complex (*Discussion*). Nevertheless, both were within the same order of magnitude (Table S3). In particular, mutant E122C, which has a 10-fold reduced ATP sensitivity and shows the slowest desensitization of these mutants on application of 10 μM ATP, also has the slowest fluorescence change. As expected, the desensitization, as determined by the fluorescence change, became faster if a saturating ATP concentration (100 μM) was used (Table S3).

Positions of the Cys Substitutions in a P2X1 Homology Model. The investigated amino acid sequence varies considerably in both length and sequence between the seven P2X subunits. To obtain an idea about the dimensions of the supposed ATP binding site and the distance and orientation of the cys-rich head domain in the P2X1R, we generated homology models for each of the aforementioned P2X1 mutants using the crystal structure of the zP2X4R as a template. In these models, the stretch between C117 and C126 forms a loop that reaches over the ATP binding site and all introduced cysteines except for E119C are predicted to be solvent-accessible (Fig. 3*A*). In agreement with the experimental data, docking of TMRM to the individual cysteine mutants (Fig. 3 *B* and *C*) revealed at least two poses that should allow the reaction with the side chain for all models except for the solvent-inaccessible E119C mutant and the A118C mutant, in which only one pose was identified. To further interpret our data, we measured the distance between the maleimide moiety of the docked TMRM and residue F188 (homologous to residue L186 in the P2X2R) as a marker for the ATP binding site (11). This measurement takes into account the flexibility of TMRM that should explore a cone in space after being fixed to the receptor and thus, gives a rough idea of possible interactions of TMRM
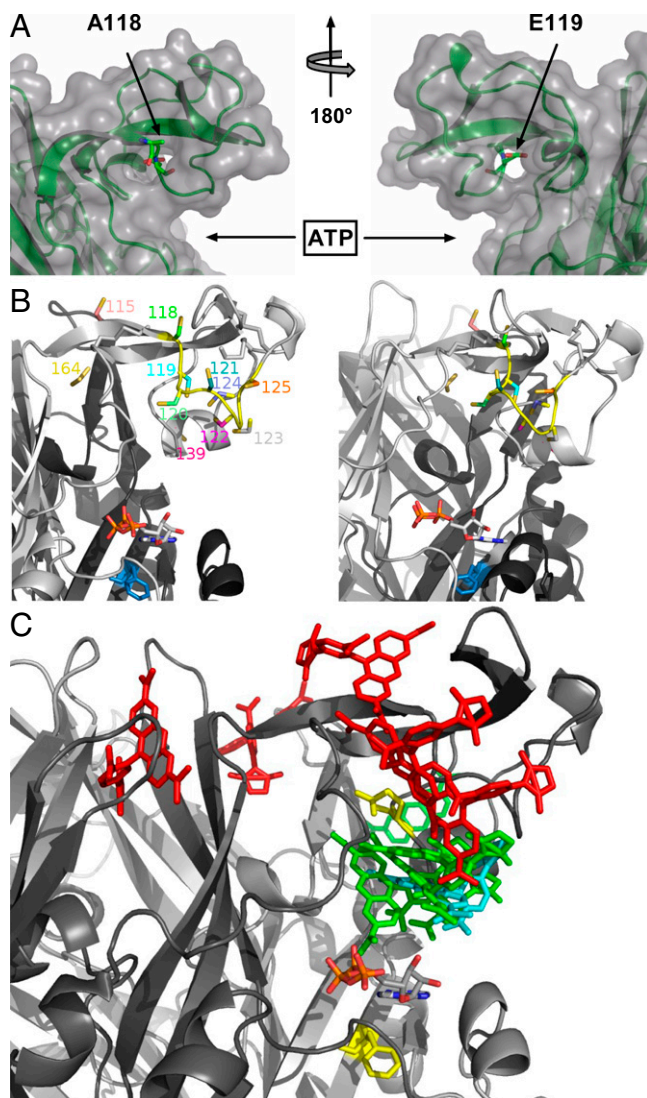
Fig. 3. Homology and docking models of the P2X1 receptor. (A) Surface representation of the head domain showing the position of the TMRM-inaccessible A118C and E119C residues. (B) Model of the proposed intersubunit ATP binding site showing the TMRM-accessible cysteine-substituted residues. ATP was docked in the proximity of F188 (blue). This constraint was used, because the docking was not robust because of the large binding site. (C) Model of the cys-rich P2X1 head domain with docked TMRM and ATP. TMRM docked to residues that were associated with ligand binding and desensitization are presented in green and red, respectively. TMRM bound to residue 124 is shown in cyan. Residues Q142 and F188 (homologous to P2X2 N140 and L186 identified by affinity labeling) are in yellow.

with the ligands. As seen in Fig. 3C and Table 1, two groups could be differentiated based on the functional and docking data: (i) mutants N120C, E122C, and G123C with a large TNP-ATP–induced fluorescence, fast decreasing signal with Bz-ATP, and distances below 21 Å and (ii) mutants P121C and I125C with small or no TNP-ATP–induced fluorescence changes, slow increasing signals with agonists, and distances above 26 Å. In contrast to the good correlation between functional and in silico data found for these mutants, unexpected results were obtained with the G124C mutant. Despite the fact that the 124C residue showed clear TMRM labeling and the model showed convincing poses for TMRM docking in a distance less than 20Å from the F188 residue, no fluorescence changes were observed on TNP-ATP binding (Fig. 2G), suggesting that the residue does not interact with ligands. In contrast to the ATP-induced

fluorescence increases of the P121C and I125C mutants, however, these changes were fast, indicating that they report channel opening.

**Additional Validation of the Model and Differentiation of Fluorescence Changes Associated with Ligand Binding, Channel Opening, and Desensitization.** Because most investigated residues are close to the ligand binding site, it is difficult to exclude that a change in TMRM fluorescence intensity is caused by or affected by quenching of the fluorophore by the ligand. To clearly isolate fluorescence changes associated with protein movements only and further validate our model, we generated three more mutants in or close to the cys-rich domain (Fig. 3). In the W164C mutant, just before the last cysteine in the cys-rich domain, the cysteine residue is predicted to face away from the ATP binding site. In agreement with this finding, this mutant showed no significant signal with TNP-ATP but a slow fluorescence increase with ATP (Fig. 4A and Fig. S5). Thus, it most likely reports the desensitization movement of the head domain only. The mutation G115C (Fig. 4B) lies two residues before the first cysteine residue of the cys-rich head domain and according to our model, over 30 Å away from residue F188 that is used as marker for the ATP binding site. As expected, it showed no fluorescence change with TNP-ATP. However, it revealed a fast fluorescence increase with ATP and therefore, most likely reports channel opening. A third mutation, R139C, was generated in the middle of the cys-rich domain, being located at a similar distance from residue F188 as the N120C, E122C, and G123C mutations and accordingly, produced virtually identical fluorescence changes with TNP-ATP (Fig. 4C) and Bz-ATP (Table S3). In further support of our hypothesis that these fluorescence changes are, at least partly, caused by direct quenching by the ligand, small or no fluorescence changes with TNP-ATP were observed with five of six (L80C, I144C, K221C, S245C, F297C, and N303C) additional control mutants in regions distant from the ligand binding site (Fig. S6). In the S245C mutant, fluorescence changes of 4.4 ± 0.8% were observed for TNP-ATP. However, this change is clearly smaller than the changes observed for the N120C, E122C, and G123C mutants and suggests movement of this protein domain during ligand binding.

Discussion

In this study, we used VCF to determine amino acid residues in the fast desensitizing P2X1R that monitor ligand binding and conformational changes during channel opening and desensitization. Based on the findings summarized in Table 1 and discussed below, we conclude that the cys-rich head domain undergoes substantial movements during P2X1R opening and desensitization. In addition, we show that the substituents at the ribose moiety of the ATP analogous ligands Bz-ATP and TNP-ATP are specifically detected by TMRM attached to position 122 and thus, provide evidence that this part of the ATP molecule is solvent-accessible rather than buried inside the ATP binding cleft. Finally, our results confirm that the intersubunit pockets seen in the crystal structure indeed represent the ATP binding sites (11, 17).

Correlation of Fluorescence Time Courses with Channel Activation and Desensitization. The simplest P2XR activation scheme leads from the resting closed (R) state through the agonist bound closed state (C) and agonist-activated open state (O) to the desensitized closed receptor (D):

$$\text{(a)} \qquad \text{(b)} \qquad \text{(c)}$$
$$R + ATP \leftrightarrow C(ATP) \leftrightarrow O(ATP) \leftrightarrow D(ATP).$$
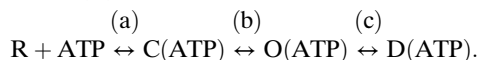
While the current signals indicate the functional states of the receptor (closed/open), changes in fluorescence can also report electrically silent ligand interactions or structural rearrangements in the protein. We propose that different mutants sense conformational changes correlating with distinct transitions (a, b, and c) in the above scheme. The fact that the fluorescence changes in mutants G115C, N120C, G123C, and G124C begin simultaneously with the currents and reach steady state by the time that the current responses reach their peak values implies that these changes

Table 1. Summary of fluorescence changes and modeling data

	115C	120C	121C	122C	123C	124C	125C	139C	164C
ATP	⇑ Fast	⇓ Fast	⇑ Slow	⇑ Slow	⇓ Fast	⇑ Fast	⇑ Slow	⇓ Fast	⇑ Slow
Bz-ATP	⇑ Fast	⇓ Fast	⇑ Slow	⇓ Fast	⇓ Fast	⇑ Fast	⇑ Slow	⇓ Fast	⇑ Slow
TNP-ATP	Small	Large	Small	Large	Large	—	Small	Large	—
Distance (Å) maleimide									
To F188	31.7	20	29.3	20.4	17.2	19.6	26.7	20.8	21.7
To K68	28.4	19.6	29.3	21.1	18.8	20.6	27.7	20.9	18.7
Reported process	2	1/2	3	1/3	1/2	2	3	1/2	3

Reported processes refer to (1) ligand binding, (2) channel opening, and (3) desensitization. Small and large responses are below 4% and above 10%, respectively. Note that the distance for W164C is misleading, because the side chain points away from the ligand binding site. Ability to detect ligand binding is dependent on quenching efficiency of the ligand. ⇑ and ⇓ indicate ΔF increase and decrease, respectively.

correlated directly with ligand binding and/or conformational changes induced by ligand binding (induced fit) and/or conformational changes during opening of the ion channel pore (a or b). The delayed (compared with the current) and slower changes in mutants P121C and I125C seemed to report subsequent movements, most likely desensitization of the receptor (c). The unclear correlation of time constants and in some cases, complex kinetics of the fluorescence changes (e.g., smaller changes in opposite direction of the dominant signal that were regularly observed with some of these mutants such as I125C) imply that parallel processes (onset of desensitization while some receptors are still activating, ligand interactions) are reported to different extents. This is also suggested by the shift in the fluorescence time constant of the P121C mutant on shorter ATP application (Fig. S2*A* and Table S3) and would be expected because of the close distance of the mutated loop to the binding site and the high flexibility of the whole loop domain. Additionally, recordings might be compromised by the limited speed of solution exchange in the VCF setup (*SI Materials and Methods*) and the fact that more channels are recorded electrophysiologically than are imaged (Fig. S2*B*). However, a clear and reproducible distinction between fast (a and b) and slow responses (c) is possible.

Specificity of Results/Antagonist Data. We used the competitive antagonist TNP-ATP to further discriminate between fluorescence changes that were caused by ligand-induced fluorophore quenching (a) and conformational changes associated with channel opening (b) and/or desensitization (c). Mutants G115C, P121C, G124C, I125C, and W164C as well as six control mutants showed comparably small (2.3–4.4%) or no fluorescence changes with TNP-ATP. All other mutants revealed large fluorescence decreases (13.5–43.4%) in the following rank order: E122C > R139C > N120C > G123C. These amplitudes are unusually high, which would be expected in the case of a direct interaction between the TMRM and the strongly quenching TNP moiety. In support of this hypothesis, a similar rank order of fluorescence

changes and increased fluorescence amplitudes compared with the full agonist ATP (2.7–5.1%) were observed with the partial agonist Bz-ATP (5.4–12.4%), which also carries an aromatic substitution at the ribose moiety and is able to efficiently quench the TMRM fluorescence. Furthermore, the rank order of quenching efficiencies of ligands reflected the amplitudes of the ligand-induced fluorescence decreases at these mutants (Fig. S4). We, therefore, propose that residues R139C, N120C, E122C, and G123C detect mainly ligand binding (a) in the case of Bz-ATP and TNP-ATP. Because ATP did not quench, the fluorescence changes observed with ATP are caused by protein movements.

We cannot exclude that TNP-ATP also induces conformational changes (e.g., induced fit) during ligand binding (a). In fact, TNP-ATP caused clear fluorescence changes in mutant S245C that is at least 25 Å away from the supposed ligand binding site, and it has even been shown to act as an agonist at a P2X2 mutant with facilitated channel gating (16). The small fluorescence changes observed with mutants P121C and I125C might also reflect such movements. In contrast, these same mutants and the more distant W164C mutant showed clear fluorescence changes with all agonists, thus further showing that they report primarily protein movements and that substantial movements of the head domain occur during channel desensitization. Likewise, the absence of significant TNP-ATP fluorescence changes in the distant G115C mutant and the G124C mutant suggests that no direct interaction with the ligand occurs. These mutants showed fast agonist-induced fluorescence changes, indicating that they report movements of the head domain associated with channel opening (b). A potential explanation for the unexpected absence of TNP-induced fluorescence change with the G124C mutant could be that the attached TMRM does not experience a shift in the dielectric constant because it interacts with a different part of the ligand or because two parallel effects that cause an increase and a decrease in fluorescence (e.g., moving away from a quenching residue and towards a quenching residue) occur at the same time. Also, it has to be considered that the distances to the ligand binding site in
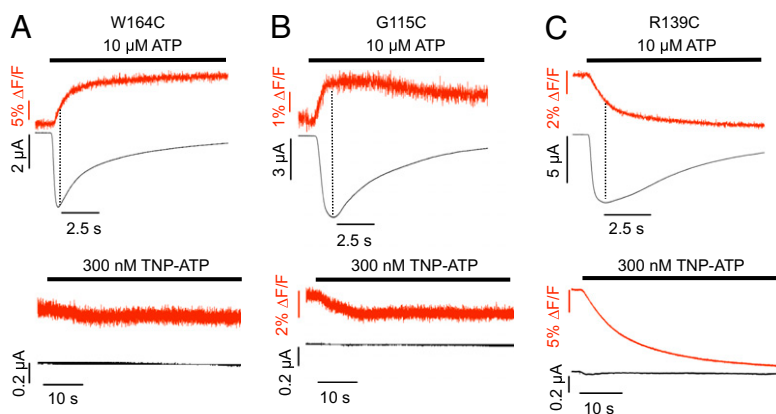

Fig. 4. Current traces and fluorescence changes of TMRM-labeled mutants that were rationally planned based on a homology model. Recordings were made on application of agonist (10 μM ATP) or antagonist (300 nM TNP-ATP). (*A*) W164C, (*B*) G115C, and (*C*) R139C. Dotted lines indicate the current peak times.

our homology model were measured from the maleimide moiety, and specific directions of the fluorescent TMR part were not considered. Thus, it is also possible that the tilt of the C124 side chain compared with the neighboring G123 residue is enough to prevent the interaction.

Homology Modeling and Docking of ATP. Our P2X1 homology model is largely supported by the experimental data. Docking studies with ATP have been difficult because of the large dimensions of the cleft supposed to constitute the ATP binding site. The location of ATP in our docking model is supported by the finding that mutants N120C and R139C, which are located at two ends of the head domain, show almost identical fluorescence changes both in quality and quantity, suggesting similar interactions with the ligands. In support of this model, the cysteine side chains introduced in these mutants are oriented to residue F188, and their distance to this residue is almost identical.

Our data imply an ATP binding mode in which its ribose moiety faces the solution and the head domain. Such an orientation of ATP is compatible with a P2X2 docking model that was determined based on the covalent attachment of NCS-ATP to residue L186 of the receptor (11). Our model also supports a docking model for Bz-ATP in the human P2X1R binding site, which has been proposed based on substituted cysteine accessibility studies (17) and in which the Bz-Bz moiety faces towards the head domain. However, these models are based on the closed receptor conformation. Our results clearly show an agonist-induced movement of the head domain, which we suggest moves down to ATP. This suggestion has also been proposed by two independent reports (18, 19), and was confirmed by the crystal structure of the ATP-bound zP2X4R (20), which were published while this work was under revision. The zP2X4 structure also fully justifies restriction of ATP binding to residue F188 in our P2X1 model. Additional studies are needed to identify the amino acid residues that transmit this movement to the transmembrane domains and the specific mechanism causing closure of the channel during desensitization.

Conclusion

In summary, using VCF, we showed that the cys-rich head domain is involved in both channel activation and desensitization. In addition, we confirmed the proposed localization of the ATP binding site and not only identified additional residues close to the ATP binding site but also determined positions that could specifically differentiate between ATP analogs. Use of this method on receptor subtypes with different pharmacology, pore opening,

and desensitization behavior will help to validate homology and docking models and contribute to elucidation of the channel activation and desensitization process and the determinants of subtype-specific ligand binding.

Materials and Methods

cDNA Constructs and cRNA Synthesis. Construction of the His-tagged rat P2X1R and mutants has been described (3, 7). Capped RNA was synthesized with the SP6 Message Machine kit (Ambion).

Oocyte Injection and Protein Labeling. *X. laevis* oocytes were prepared and labeled with Cy5 *N*-hydroxysuccinimide ester as described (3, 7). For cysteine-specific fluorescence labeling, oocytes were incubated for 15 min in the dark and on ice in 5 μM TMRM (Molecular Probes) in ND96. Oocytes were subsequently washed and extracted or kept on ice (<1 h) until used for recording.

Purification of Hexahistidyl-Tagged Proteins and SDS/PAGE. Protein complexes containing His-tagged P2X subunits were purified from dodecylmaltoside extracts of *Xenopus* oocyte, separated by SDS/PAGE, and analyzed as described (3, 7).

Electrophysiological Recordings. Two-electrode voltage clamp recordings at −60 mV were performed as described (7, 14) using a TEC-05 amplifier (NPI Electronics), low pass filtered at 100 Hz, and sampled at 200 Hz. VCF recordings were performed principally as described (21) using an Axiovert 200 inverted fluorescence microscope equipped with a 20× Neofluar objective (N.A. = 0.75, working distance = 2 mm) and the BP545/25, FT570, BP605/70 filter set (Carl Zeiss MicroImaging). Fluorescence was recorded with a Hamamatsu SN5973 photodiode and an FDU-2 fluorescence detection unit mounted to the bottom port (Till Photonics). Data were recorded with CellWorks software (NPI Electronic) and analyzed with Origin 7.5 software (Microcal).

Homology Modeling. Models for each P2X1 mutant were prepared as described (11) using the program Modeler 9v9 (22) and analyzed for solvent accessibility with the DSSP software (23). Docking was performed with Autodock vina software (24) using a distance below 5 Å between the thiol group and the maleimide moiety and correct side chain orientation as constraints. Figures were prepared with PyMOL (DeLano Scientific LLC).

1. Surprenant A, North RA (2009) Signaling at purinergic P2X receptors. *Annu Rev Physiol* 71:333–359.
2. Kawate T, Michel JC, Birdsong WT, Gouaux E (2009) Crystal structure of the ATP-gated P2X(4) ion channel in the closed state. *Nature* 460:592–598.
3. Nicke A, et al. (1998) P2X1 and P2X3 receptors form stable trimers: A novel structural motif of ligand-gated ion channels. *EMBO J* 17:3016–3028.
4. Ennion SJ, Ritson J, Evans RJ (2001) Conserved negatively charged residues are not required for ATP action at P2X(1) receptors. *Biochem Biophys Res Commun* 289:700–704.
5. Jiang LH, Rassendren F, Surprenant A, North RA (2000) Identification of amino acid residues contributing to the ATP-binding site of a purinergic P2X receptor. *J Biol Chem* 275:34190–34196.
6. Roberts JA, Evans RJ (2004) ATP binding at human P2X1 receptors. Contribution of aromatic and basic amino acids revealed using mutagenesis and partial agonists. *J Biol Chem* 279:9043–9055.
7. Marquez-Klaka B, Rettinger J, Bhargava Y, Eisele T, Nicke A (2007) Identification of an intersubunit cross-link between substituted cysteine residues located in the putative ATP binding site of the P2X1 receptor. *J Neurosci* 27:1456–1466.
8. Marquez-Klaka B, Rettinger J, Nicke A (2009) Inter-subunit disulfide cross-linking in homomeric and heteromeric P2X receptors. *Eur Biophys J* 38:329–338.
9. Pless SA, Lynch JW (2008) Illuminating the structure and function of Cys-loop receptors. *Clin Exp Pharmacol Physiol* 35:1137–1142.
10. Adriouch S, et al. (2008) ADP-ribosylation at R125 gates the P2X7 ion channel by presenting a covalent ligand to its nucleotide binding site. *FASEB J* 22:861–869.
11. Jiang R, et al. (2011) Agonist trapped in ATP-binding sites of the P2X2 receptor. *Proc Natl Acad Sci USA* 108:9066–9071.
12. Clyne JD, Wang LF, Hume RI (2002) Mutational analysis of the conserved cysteines of the rat P2X2 purinoceptor. *J Neurosci* 22:3873–3880.
13. Ennion SJ, Evans RJ (2002) Conserved cysteine residues in the extracellular loop of the human P2X(1) receptor form disulfide bonds and are involved in receptor trafficking to the cell surface. *Mol Pharmacol* 61:303–311.
14. Rettinger J, Schmalzing G (2003) Activation and desensitization of the recombinant P2X1 receptor at nanomolar ATP concentrations. *J Gen Physiol* 121:451–461.
15. Roberts JA, Evans RJ (2007) Cysteine substitution mutants give structural insight and identify ATP binding and activation sites at P2X receptors. *J Neurosci* 27:4072–4082.
16. Cao L, Young MT, Broomhead HE, Fountain SJ, North RA (2007) Thr339-to-serine substitution in rat P2X2 receptor second transmembrane domain causes constitutive opening and indicates a gating role for Lys308. *J Neurosci* 27:12916–12923.
17. Allsopp RC, El Ajouz S, Schmid R, Evans RJ (2011) Cysteine scanning mutagenesis (residues Glu52-Gly96) of the human P2X1 receptor for ATP: Mapping agonist binding and channel gating. *J Biol Chem* 286:29207–29217.
18. Roberts JA, et al. (2012) Agonist binding evokes extensive conformational changes in the extracellular domain of the ATP-gated human P2X1 receptor ion channel. *Proc Natl Acad Sci USA* 109:4663–4667.
19. Jiang R, et al. (2012) Tightening of the ATP-binding sites induces the opening of P2X receptor channels. *EMBO J* 31:2134–2143.
20. Hattori M, Gouaux E (2012) Molecular mechanism of ATP binding and ion channel activation in P2X receptors. *Nature* 485:207–212.
21. Mourot A, Bamberg E, Rettinger J (2008) Agonist- and competitive antagonist-induced movement of loop 5 on the alpha subunit of the neuronal alpha4beta4 nicotinic acetylcholine receptor. *J Neurochem* 105:413–424.
22. Sali A, Blundell TL (1993) Comparative protein modelling by satisfaction of spatial restraints. *J Mol Biol* 234:779–815.
23. Kabsch W, Sander C (1983) Dictionary of protein secondary structure: Pattern recognition of hydrogen-bonded and geometrical features. *Biopolymers* 22:2577–2637.
24. Trott O, Olson AJ (2010) AutoDock Vina: improving the speed and accuracy of docking with a new scoring function, efficient optimization, and multithreading. *J Comput Chem* 31:455–461.

PHARMACOLOGY